Jahn-Teller effect in C H 3 D + and C D 3 H + : Conformational isomerism, tunneling-rotation structure, and the location of conical intersections

H. J. Wörner and F. Merkt

Citation: The Journal of Chemical Physics **126**, 154304 (2007); doi: 10.1063/1.2716394
View online: http://dx.doi.org/10.1063/1.2716394
View Table of Contents: http://scitation.aip.org/content/aip/journal/jcp/126/15?ver=pdfcov
Published by the AIP Publishing

Jahn-Teller effect in CH_3D^+ and CD_3H^+: Conformational isomerism, tunneling-rotation structure, and the location of conical intersections

H. J. Wörner and F. Merkt
Laboratorium für Physikalische Chemie, ETH-Zürich, 8093 Zürich, Switzerland

(Received 11 January 2007; accepted 20 February 2007; published online 16 April 2007)

High-resolution pulsed-field-ionization zero-kinetic-energy photoelectron spectra of CH_3D and CD_3H have been recorded at rotational resolution from the adiabatic ionization energy up to 600 cm^{-1} of internal energy of the respective cations. The spectra are characterized by the effects of a large-amplitude pseudorotational motion exchanging the equivalent nuclei in each molecule. With increasing internal energy, a transition from the tunneling regime with splittings of the order of $1-10$ cm^{-1} to the free pseudorotation regime is observed. A theoretical model that treats the simultaneous rotational and pseudorotational motions and incorporates the effects of the geometric phase has been developed. The model provides the appropriate rovibronic symmetries in the $C_{3v}(M)$ molecular symmetry group and reaches a near-quantitative agreement with the experimental data. The complete group-theoretical analysis of the rovibronic problem is also given. The analysis of the spectra has revealed the existence of two different isomers for both CH_3D^+ and CD_3H^+, which differ in the bond length between the carbon atom and the unique ligand atom. All isomers are subject to a fast pseudorotational motion between three equivalent minima with a period of $3-5$ ps in CH_3D^+ and $18-28$ ps in CD_3H^+. The analysis has also provided the ordering of the tunneling sublevels for each isomer, which enables the location of the twofold conical intersections on the potential energy surface that could not be determined from experiments on CH_4^+. © *2007 American Institute of Physics*. [DOI: 10.1063/1.2716394]

I. INTRODUCTION

Isotopic substitution is one of the most elegant and useful methods in the investigation of the structure and dynamics of molecular systems. Partial isotopic substitution reduces the symmetry of the normal vibrations without affecting the electronic symmetry properties. It is therefore particularly valuable in the investigation of systems that are subject to vibronic coupling because the electronic and nuclear dynamics are strongly correlated in these systems. Isotopic substitution is also helpful in understanding the properties of molecules performing large-amplitude motions because it reduces the permutational symmetry and introduces asymmetries in the potential energy surface through vibrational zero-point effects.

Partial substitution of molecules subject to a Jahn-Teller (JT) effect[1,2] has been considered theoretically for the $E\otimes e$ problem[3,4] and its spectroscopic consequences were studied by electron paramagnetic resonance (EPR) in the cyclooctatetraene anion[5] and the benzene anion[6] and by optical spectroscopy in benzene[7] and the cyclopentadienyl radical.[8] All investigated systems possess a doubly degenerate ground electronic state that is subject to a dominantly linear interaction with some vibrational modes. In the case of benzene and cyclopentadienyl, the dominantly linear JT effect leads to a potential energy surface with a cylindrically symmetric trough,[9,10] which is occasionally referred to as "Mexican hat." The weaker quadratic JT effect leads to minima along the trough connected by small to vanishing barriers. In these systems, partial deuteration leads to the appearance of one minimum on the potential energy surface that corresponds to the most favorable structure. In the case of cyclopentadienyl, the barriers between the equivalent minima vanish by symmetry[11] and both C_5H_4D and C_5D_4H possess a single minimum on the lowest potential energy surface. An additional effect of partial deuteration is the splitting of the lowest vibronic level of symmetry E_1'' in D_{5h} into two components of symmetries A_2 and B_1 in C_{2v}. In the case of several excited electronic states of benzene and of the ground state of the benzene anion, quadratic coupling is weak and leads to very small barriers between the equivalent minima.[6] These minima are not deep enough to support localized nuclear wave functions and therefore single deuteration also leads to a single preferred geometry of the molecule that was identified in the EPR experiments. The effects of partial deuteration in the systems mentioned above can be summarized as a transition from a situation where pseudorotation takes place to a static JT distortion since vibrational zero-point effects result in a single preferred geometry of the molecule.

The situation is quite different in the methane cation which is the topic of this article. The methane cation is the prototypical system for the $T\otimes(e+t_2)$ JT effect. In this system strong quadratic coupling leads to 12 equivalent minima of C_{2v} symmetry that are separated by high barriers.[12] The effect of partial isotopic substitution on JT systems with deep minima has not been investigated before but the emergence of new isotopic effects has been anticipated by Applegate *et al.*: "…there is the intriguing possibility of Jahn-Teller molecules being isolated sufficiently long in distorted geometries to exhibit strongly different chemical reactivity."[13] A C_{2v} minimum energy structure has been first predicted for CH_4^+

by Meyer[14] and has been confirmed by more recent *ab initio* quantum chemical calculations.[12,15,16] The C_{2v} minimum energy structure has been verified experimentally from the determination of the symmetries of the tunneling sublevels of the ground state in a rotationally resolved photoelectron spectrum.[17] This study has also shown that the hydrogen atoms exchange with a period of 2.1(5) ps, i.e., on a time scale similar to that of molecular rotation. CH_3D^+ and CD_3H^+ have been studied by EPR,[18] which has revealed that the three protons of CH_3D^+ and the three deuterons of CD_3H^+ are equivalent on the time scale of the experiment. The same study has shown that the four protons in CH_4^+ are also equivalent on that time scale but that, in $CH_2D_2^+$, the protons and deuterons must occupy different sites. The conclusion on $CH_2D_2^+$ was subsequently confirmed by the analysis of a rotationally resolved photoelectron spectrum,[19] which proved that $CH_2D_2^+$ possesses two equal C–H bonds that are longer than the two equal C–D bonds.

A previous investigation of CH_4^+, CD_4^+, CH_3D^+, and $CH_2D_2^+$ by pulsed-field-ionization zero-kinetic energy (PFI-ZEKE) photoelectron spectroscopy[20] has provided a qualitative understanding of the dynamics of these molecules at low excitation energies using a one-dimensional model for the large-amplitude pseudorotational motion. The model was, however, incapable of reflecting the full symmetry of the problem because of its reduced dimensionality, and neither the vibronic nor the rovibronic symmetries could be predicted correctly. Moreover, the model did not incorporate the effects of the geometric phase and has underestimated the size of the tunneling splittings. Very recently, the lowest bands in the PFI-ZEKE spectra of CH_4^+ and CD_4^+ have been reanalyzed using a tunneling treatment that reflects the full permutational symmetry and also includes the effect of the geometric phase. This analysis led to the assignment of the rotational structure of the spectrum.[17,21] In the present article, the PFI-ZEKE photoelectron spectrum of CD_3H^+ is reported for the first time and a complete analysis of the tunneling-rotation structure of CH_3D^+ and CD_3H^+ at low energies is presented. The analysis required the extension of the model introduced in Ref. 17 to treat the tunneling-rotation structure of partially deuterated species.

II. EXPERIMENT

The photoion/photoelectron spectrometer and the vacuum-ultraviolet (vuv) light source used in the present experiments have been described previously.[22] CH_3D and CD_3H (Cambridge Isotope Laboratories, 98% chemical purity, 98% isotopic enrichment) were introduced into the spectrometer in a pulsed supersonic expansion of a 1:1 mixture with argon (stagnation pressure of 2–3 bars, 10 Hz repetition rate). vuv radiation was generated by two-photon resonance-enhanced sum-frequency mixing ($\nu_{vuv}=2\nu_1+\nu_2$) of the output of two Nd:YAG-pumped dye lasers (YAG stands for yttrium aluminum garnet) in Xe using the $(5p)^5 6p[1/2]_0 \leftarrow (5p)^6\ ^1S_0$ two-photon resonance at $2\tilde{\nu}_1 = 80\,118.964\ cm^{-1}$. The vuv radiation was separated from the fundamental beams in a vacuum monochromator using a toroidal dispersion grating which also recollimated the diverging vuv beam and redirected it toward a photoexcitation-photoionization chamber where it intersected the molecular beam at right angles.

PFI-ZEKE photoelectron spectra were recorded by monitoring the pulsed electric field ionization of high Rydberg states located immediately below the ionization thresholds as a function of the laser wave number. A positive pulsed electric field of less than 1 V/cm and of 1 μs duration was applied 1 μs after photoexcitation and was immediately followed by a negative pulsed electric field of comparable amplitude. The first (discrimination) pulse served the purpose of removing prompt electrons and of ionizing the highest Rydberg states. The PFI-ZEKE spectra were obtained by recording the field-ionization yield of the second pulse. Photoionization spectra were measured by recording the ion yield as a function of the laser wave number, which was calibrated as described in Ref. 21.

III. THEORY

A. The potential energy surfaces

Partial isotopic substitution of methane lowers the symmetry of the normal vibrations but leaves the electronic symmetry properties unchanged. Therefore, the topological relations between the minima and saddle points on the potential energy surfaces of CH_4^+ (Refs. 12 and 15) are conserved upon deuteration. The minimum energy structure of CH_4^+ has a C_{2v} geometry,[12,14–17,21] two C–H bonds being elongated (1.186 Å) and two bonds shortened (1.098 Å) compared to the tetrahedral reference geometry. The long bonds form an angle of 55° that is substantially smaller than the tetrahedral angle and the short bonds enclose an increased angle (126°). These structural parameters were obtained by optimizing the geometry of the methane cation at the CCSD(T)/cc-pVTZ level of *ab initio* theory.[21] In CH_4^+, distortion from the tetrahedral geometry leads to six equivalent C_{2v} structures which are connected by 12 equivalent first-order saddle points of C_s symmetry. A cyclic exchange of three hydrogen atoms, which is often referred to as "pseudorotation,"[12] transforms one minimum energy structure to an equivalent one and the corresponding minimum energy path leads through the C_s saddle point. An additional set of six minima and 12 saddle points is obtained by inverting the molecule. The topology of the potential energy surface is represented schematically in Fig. 1, which represents the distorted structures of CH_3D^+. The center of the triangular faces of the octahedron corresponds to structures of C_{3v} symmetry in CH_4^+. Two types of triangular faces can be distinguished depending on whether a short or a long C–H bond (the C–D bond in the figure) is conserved in the motion encircling that face. In the former case, the center of the triangular face corresponds to a structure of C_{3v} geometry with one short C–D and three long C–H bonds. This structure possesses a doubly degenerate lowest electronic state and a nondegenerate excited state,[15] both arising from the threefold degenerate $^2F_2$ state of CH_4^+ at the tetrahedral reference geometry. The position of this structure in configuration space is indicated by a dot in Fig. 1. The other four triangular faces correspond to a structure of C_{3v} geometry with a long C–D and three short C–H bonds pos-

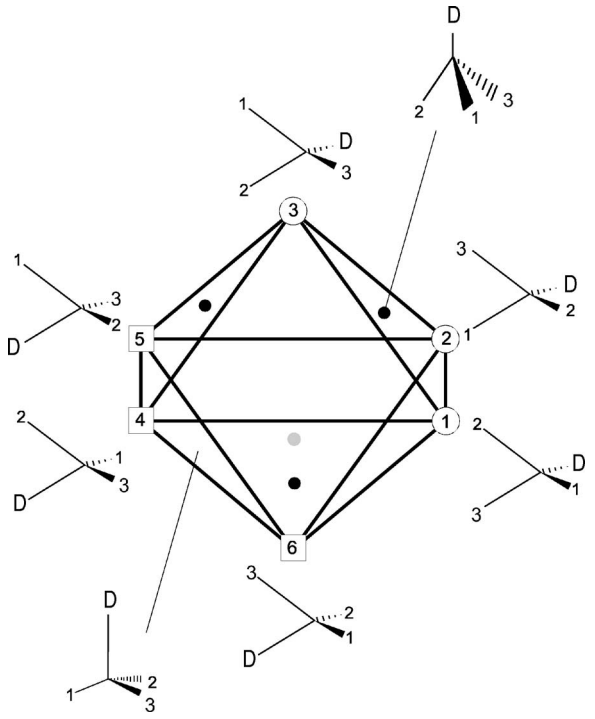

FIG. 1. Schematic representation of several stationary points on the potential energy surface of CH_3D^+ and their topological relationships. The empty circles correspond to the three equivalent minima of the more stable isomer $CH_3D_s^+$. The squares represent the three equivalent minima of the isomer $CH_3D_\ell^+$. The filled circles on four faces of the octahedron represent the C_{3v} structures possessing a doubly degenerate ground electronic state and the center of the remaining four faces correspond to the C_{3v} structures with a nondegenerate ground state. The structure of the C_{2v} and C_{3v} stationary points that are of importance in the present study are depicted.

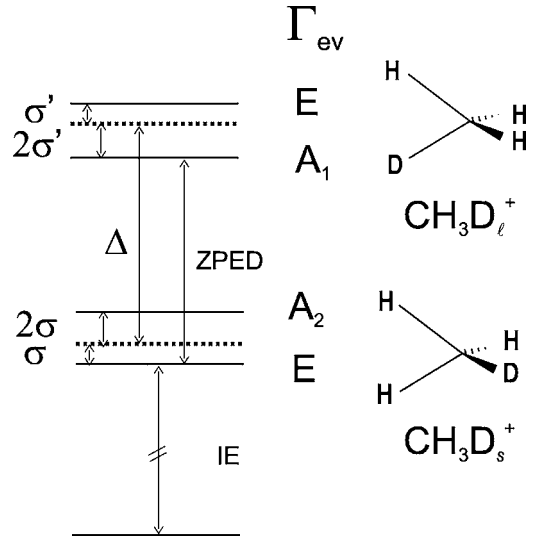

FIG. 2. Tunneling levels of CH_3D^+ with zero total angular momentum and ground vibronic state of CH_3D (full lines). The quantities σ and σ' represent the tunneling integrals for the isomers $CH_3D_s^+$ and $CH_3D_\ell^+$, respectively, ZPED stands for the zero-point energy difference between these isomers, and IE is the adiabatic ionization energy. Δ describes the zero-point energy difference in the absence of tunneling.

sessing a nondegenerate ground electronic state and a doubly degenerate excited state.[15]

The potential energy surfaces of CH_4^+ can be interpreted in terms of a $T_2 \otimes (e+2t_2)$ JT effect. The associated eight-dimensional hypersurfaces are complex but their topological relationship is easily understood from a decomposition into two consecutive distortions, which is also very useful in understanding the JT effect in the partially deuterated isotopomers. We assume first that CH_4^+ is distorted along a linear combination of the two modes of symmetry f_2 to the C_{3v} structure indicated by a dot in Fig. 1 with one short C–H bond and a doubly degenerate ground state. A second distortion along the e mode (in T_d), which has the same irreducible representation in C_{3v}, leads to one of the three C_{2v} minima located at the corners of the corresponding face of the octahedron, e.g., structures 1, 2, and 3 in Fig. 1. This second distortion corresponds exactly to the well-known $E \otimes e$ JT effect of a molecule of C_{3v} (or D_{3h}) symmetry in a doubly degenerate ground state, which leads to three equivalent minima connected by three equivalent saddle points.[9,10,23] The motion connecting the three structures around a triangular face thus encircles a conical intersection. Alternatively, CH_4^+ can be distorted to a C_{3v} structure with one long C–H bond and a nondegenerate ground state. The second distortion along an e mode also leads to three C_{2v} minima, e.g., structures 4, 5, and 6 in Fig. 1, but the local topology of the potential surfaces must be different from the case discussed previously. The lowest surface is nondegenerate, but the vibronic coupling to the degenerate excited state leads to a stabilization of the lower surface upon distortion that results from an $(A_1 \oplus E) \otimes e$ pseudo-JT effect. Hence, the motion around a triangular face of this kind does not encircle a point of electronic degeneracy.

Although deuteration does not affect the properties of the electronic surfaces, it has a profound impact on the dynamics of molecules through vibrational zero-point energy effects. Single or triple deuteration of CH_4^+ lifts the high permutational symmetry of the system and reduces the number of equivalent minimum energy structures from six to two sets of three structures. After applying the zero-point correction to the potential energy surface, a structure of CH_3D^+ with the D atom on a long bond is no longer isoenergetic with a structure that has a short C–D bond. This effect is illustrated in Fig. 1 where the local minima 1, 2, and 3 corresponding to a structure with a short C–D bond are indicated by circles and those corresponding to a long C–D bond by squares (4, 5, and 6). A similar situation is encountered in CD_3H^+ which possesses two sets of three equivalent structures. *Ab initio* calculations of the vibrational frequencies show that the zero-point effects favor those structures where a maximum number of deuterium atoms are located on short bonds. This result is in agreement with the intuitive expectation that short bonds correspond to large force constants, which cause the largest zero-point effects. Harmonic zero-point energy differences between the two possible structures amount to 114 cm^{-1} in CH_3D^+ and 107 cm^{-1} in CD_3H^+ at the CCSD(T)/cc-pVTZ level of theory. As will be demonstrated below, the two sets of structures (1,2,3) and (4,5,6) represent two isomeric forms of CH_3D^+ (and CD_3H^+) which are displayed on the right-hand side of Figs. 2 and 3. These isomers are labeled $CH_3D_s^+$ ($CD_3H_\ell^+$) and $CH_3D_\ell^+$ ($CD_3H_s^+$), where the subscripts s and ℓ indicate that the single ligand

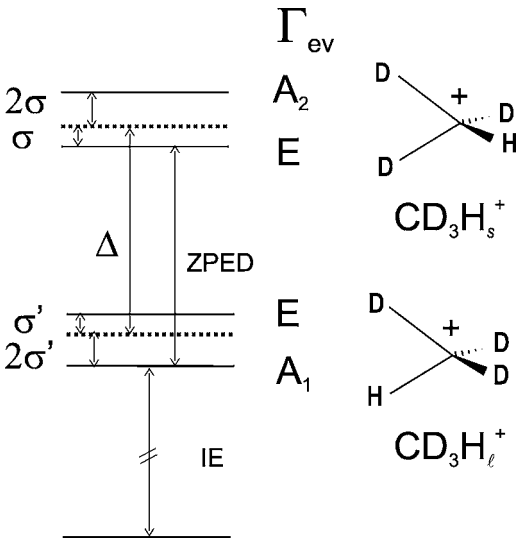

FIG. 3. Tunneling levels of CD_3H^+ with zero total angular momentum and ground vibronic state of CD_3H (full lines). The quantities σ and σ' represent the tunneling integrals for the isomers $CD_3H_\ell^+$ and $CD_3H_s^+$, respectively, ZPED stands for the zero-point energy difference between these isomers, and IE is the adiabatic ionization energy. Δ describes the zero-point energy difference in the absence of tunneling.

atom lies on a short or a long bond, respectively.

The molecular symmetry group $C_{3v}(M)$ contains permutation-inversion operations of the type E, (123) and $(12)^*$, which are all feasible if the splittings resulting from the pseudorotational motion are observable. We will therefore use the $C_{3v}(M)$ group to describe the symmetry of the rovibronic levels of CH_3D^+ and CD_3H^+.

B. The tunneling problem

The tunneling motion between the six equivalent minima of CH_4^+ and CD_4^+ in the rotationless ground state can be described by an effective Hamiltonian expressed in the basis

$$\phi_n = |n\rangle|\chi_n\rangle, \tag{1}$$

where $|n\rangle$ is the adiabatic electronic function in the nth potential well and $|\chi_n\rangle$ represents the ground state vibrational wave function (a product of nine harmonic oscillator functions) of the molecule in the nth potential well.[17,21] $|n\rangle$ is the eigenvector corresponding to the lowest eigenvalue of the 3×3 potential energy matrix for CH_4^+ that was derived in Ref. 15 and takes the form $\frac{1}{\sqrt{2}}(-|\xi\rangle+|\eta\rangle)$, $\frac{1}{\sqrt{2}}(-|\xi\rangle+|\zeta\rangle)$, $\frac{1}{\sqrt{2}}(|\eta\rangle-|\zeta\rangle)$, $\frac{1}{\sqrt{2}}(|\xi\rangle+|\eta\rangle)$, $\frac{1}{\sqrt{2}}(|\xi\rangle+|\zeta\rangle)$, and $\frac{1}{\sqrt{2}}(|\eta\rangle+|\zeta\rangle)$ for minima 1 through 6, where $|\xi\rangle,|\eta\rangle,|\zeta\rangle$ are the diabatic electronic wave functions of the electronic triplet in its tetrahedral reference geometry.[17]

Neglecting the overlap between the vibrational basis functions and defining $\sigma=1/2\langle\chi_1|\hat{H}_{\rm vib}|\chi_2\rangle$ and $\langle\chi_1|\hat{H}_{\rm vib}|\chi_1\rangle=0$, where $\hat{H}$ is the vibrational operator for the lowest potential energy surface, the tunneling eigenstates of CH_4^+ are obtained from the diagonalization of the Hamiltonian matrix

$$\mathbf{H}_{\rm vib}=\begin{pmatrix} 0 & \sigma & \sigma & 0 & -\sigma & \sigma \\ \sigma & 0 & -\sigma & -\sigma & 0 & \sigma \\ \sigma & -\sigma & 0 & \sigma & -\sigma & 0 \\ 0 & -\sigma & \sigma & 0 & \sigma & \sigma \\ -\sigma & 0 & -\sigma & \sigma & 0 & \sigma \\ \sigma & \sigma & 0 & \sigma & \sigma & 0 \end{pmatrix}, \tag{2}$$

which provides two sets of triply degenerate levels with eigenvalues $+2\sigma$ and -2σ, respectively, where σ is negative. The high permutational symmetry of CH_4^+ is responsible for the equality of all matrix elements $\langle\chi_i|\hat{H}_{\rm vib}|\chi_i\rangle$ and all tunneling elements $\langle\chi_i|\hat{H}_{\rm vib}|\chi_j\rangle$.

Deuteration of CH_4^+ to CH_3D^+ reduces the permutational symmetry and results in two distinct sets of three structures each that differ in zero-point energy. In addition, the 12 equivalent saddle points of C_s symmetry in CH_4^+ are split into four distinct sets of three equivalent structures. The saddle-point structures for pseudorotation among the minima of $CH_3D_s^+$ ($CH_3D_\ell^+$) have a short (long) C–D bond. The saddle-point structures possessing one H and one D atom on the equal bonds are enantiomers of each other and therefore the corresponding pseudorotation paths are equivalent. Consequently, the following matrix elements can be defined:

$$\begin{aligned} &\langle\chi_i|\hat{H}|\chi_i\rangle = 0 \quad \text{for } i\in\{1,2,3\},\\ &\langle\chi_i|\hat{H}|\chi_i\rangle = \Delta \quad \text{for } i\in\{4,5,6\},\\ &1/2\langle\chi_i|\hat{H}|\chi_j\rangle = \sigma \quad \text{for } i\neq j,\{i,j\}\in\{1,2,3\},\\ &1/2\langle\chi_i|\hat{H}|\chi_j\rangle = \sigma' \quad \text{for } i\neq j,\{i,j\}\in\{4,5,6\},\\ &1/2\langle\chi_i|\hat{H}|\chi_j\rangle = \sigma'' \quad \text{for } i\neq j, i\in\{1,2,3\},\\ &\qquad\qquad j\in\{4,5,6\} \text{ or vice versa}, \end{aligned} \tag{3}$$

where i and j refer to the structures drawn in Fig. 1 and σ, σ', and σ'' are negative. The zero-point-corrected potential energy of the more stable structures (1,2,3 for CH_3D^+, see Fig. 1) has been chosen as the origin of the energy scale. Δ represents the zero-point energy difference between the two sets of structures corresponding to minima 1–3 and 4–6 in the absence of tunneling. σ is the tunneling matrix element for the interconversion of the structures 1, 2, and 3, σ' that for structures 4, 5, and 6, and σ'' represents the interaction between vibrational basis functions localized in inequivalent minima. The tunneling matrix elements have negative values. The tunneling matrix for CH_3D^+ takes the form

$$\mathbf{H}_{\rm tun}=\begin{pmatrix} 0 & \sigma & \sigma & 0 & -\sigma'' & \sigma'' \\ \sigma & 0 & -\sigma & -\sigma'' & 0 & \sigma'' \\ \sigma & -\sigma & 0 & \sigma'' & -\sigma'' & 0 \\ 0 & -\sigma'' & \sigma'' & \Delta & \sigma' & \sigma' \\ -\sigma'' & 0 & -\sigma'' & \sigma' & \Delta & \sigma' \\ \sigma'' & \sigma'' & 0 & \sigma' & \sigma' & \Delta \end{pmatrix}, \tag{4}$$

and has the eigenvalues

$$E_E = \tfrac{1}{2}(\sigma - \sigma' + \Delta - S), \tag{5a}$$

$$E_{A_2} = -2\sigma, \tag{5b}$$

$$E_{A_1} = 2\sigma' + \Delta, \tag{5c}$$

$$E_E = \tfrac{1}{2}(\sigma - \sigma' + \Delta + S). \tag{5d}$$

In Eqs. (5a)–(5d) the subscripts correspond to the irreducible representations of the corresponding eigenvectors in $C_{3v}(M)$ and

$$S = \sqrt{(\sigma + \sigma')^2 + 12\sigma'' - 2(\sigma + \sigma')\Delta + \Delta^2}. \tag{6}$$

In the limit $(|\sigma|, |\sigma'|, |\sigma''|) \ll \Delta$ one obtains

$$S \approx \Delta - (\sigma + \sigma') + \frac{(\sigma + \sigma')^2 + 12\sigma''}{2\Delta} \approx \Delta - (\sigma + \sigma'), \tag{7}$$

and the eigenvalues converge to

$$E_E = \sigma, \tag{8a}$$

$$E_{A_2} = -2\sigma, \tag{8b}$$

$$E_{A_1} = 2\sigma' + \Delta, \tag{8c}$$

$$E_E = -\sigma' + \Delta, \tag{8d}$$

corresponding to two tunneling pairs with tunneling splittings $\delta = 3|\sigma|$ and $\delta' = 3|\sigma'|$, respectively. These tunneling states are represented schematically in Figs. 2 and 3 for CH_3D^+ and CD_3H^+, respectively. If the zero-point energy difference dominates over the value of the tunneling integrals, tunneling between inequivalent minima is suppressed by the asymmetry of the potential and one can consider the structures (1,2,3) and (4,5,6) as forming distinct isomers. The symmetry inherent to the system implies that the tunneling substates of symmetries A_1 and A_2 are entirely localized in the minima 4,5,6 on the one hand and 1,2,3 on the other, irrespective of the values of the parameters. These substates can thus always be identified with one of the isomers if their interaction with excited vibrational levels is neglected.

In an earlier publication on the tunneling dynamics in CH_4^+,[17] we have discussed the effect of the electronic degeneracies on the structure of the tunneling levels. The lowest potential energy surface of CH_4^+ contains two types of electronic degeneracies which are enforced by symmetry (additional "accidental" degeneracies also exist[24]): one conical intersection corresponding to a threefold degeneracy at the tetrahedral geometry and four conical intersections corresponding to a twofold degeneracy at the four possible C_{3v} structures with a single short C–H bond indicated by the dots in Fig. 1. When an adiabatic electronic wave function is transported in a closed loop around an odd number of conical intersections, its sign must change when the loop is completed.[9,10,25] One can indeed verify that the product of three consecutive overlaps of the adiabatic electronic wave functions in the sequence $1 \to 2 \to 3 \to 1$ is negative, whereas a positive number results from the sequence $4 \to 5 \to 6 \to 4$, where the numbers 1–6 refer to the structure labels introduced in Fig. 1. The sign change along the former loop is a direct manifestation of the presence of a conical intersection inside the former path, and the sign conservation along the latter loop results from the absence of such a degeneracy point (or an even number of them) in the latter. The topological properties of the potential surfaces are thus properly encoded in the adiabatic electronic functions. The properties of the two tunneling paths discussed here are qualitatively unchanged by single deuteration. Therefore, the ordering of tunneling levels $E_E \leqslant E_{A_2}$ in the set (1,2,3) can be interpreted as a signature of the conical intersection encircled by the corresponding tunneling motion, and the ordering $E_{A_1} \leqslant E_E$ in the set (4,5,6) represents the "normal" splitting of tunneling between three equivalent minima. This conclusion is in agreement with the interpretation given above that minima (1,2,3) arise from an $E \otimes e$ JT effect (for which the ordering $E_E \leqslant E_A$ has been established[26]) and minima (4,5,6) from an $(A \oplus E) \otimes e$ pseudo-JT effect. In conclusion, the ordering of the tunneling states in the partially deuterated isotopomers can directly be translated into topological information on the potential energy surface that cannot be obtained directly from spectra of CH_4^+ or CD_4^+.

The tunneling structure of CD_3H^+ is in many respects similar to that of CH_3D^+, but the role of the two sets of minima is exchanged. Replacing all H (D) atoms by D (H) atoms in Fig. 1 renders the set of structures 4,5,6 more stable than the set 1,2,3. The tunneling substates in order of increasing energy are in this case

$$E_{A_1} = 2\sigma', \tag{9a}$$

$$E_E = -\sigma', \tag{9b}$$

$$E_E = \sigma + \Delta, \tag{9c}$$

$$E_{A_2} = -2\sigma + \Delta, \tag{9d}$$

a situation that is schematically depicted in Fig. 3.

C. The rovibronic problem

A simple description of the rotational motion in the lowest tunneling states of CH_3D^+ and CD_3H^+ is obtained by expressing the rotational operators in an axis system that is common to all distorted structures. CH_3D^+ and CD_3H^+ both possess two sets of three equivalent minimum energy structures that differ in the value of the zero-point energy. The transformation of the axes for the distorted structure of CH_3D^+ in which the D atom is located on a short bond is represented schematically in Fig. 4. The C_{3v} equilibrium structure (a) of CH_3D is chosen as the reference geometry and the axes x, y, z are chosen along the principal inertial axes. The y axis lies in the plane containing the H_1, D, and C atoms. The molecule is then distorted to the equilibrium structure (b) of CH_3D^+ by (1) shortening the C–D and the C–H bonds lying in the yz plane, (2) increasing the corresponding (DCH) angle, (3) lengthening the two remaining C–H bonds, and (4) decreasing their (HCH) angle. The ori-

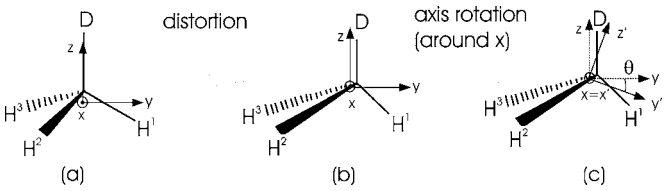

FIG. 4. Axis systems used in the derivation of the rotational Hamiltonian. The principal axis system of the neutral molecule is depicted on the left-hand side (a). After distortion of the molecule to the equilibrium structure of the cation (b), the axis system is translated to the new center of mass and then rotated about the x axis until it coincides with the principal axis system of the distorted molecule (c).

gin of the axis system is moved to the new center of gravity of the molecule. Then, the axes are rotated by an angle θ about the x axis such that they coincide with the principal axis system (x',y',z') of the distorted structure indicated in (c). In this axis system, the rotational Hamiltonian takes the form

$$\frac{\hat{H}^{(1)}_{\mathrm{rot}}}{hc} = C\hat{J}^2_{x'} + B\hat{J}^2_{y'} + A\hat{J}^2_{z'}, \tag{10}$$

where the superscript designates the minimum structure as defined in Fig. 1. Inserting the expressions for the rotational operators $\hat{J}_{x'},\hat{J}_{y'},\hat{J}_{z'}$ in terms of the operators defined in the global axis system $\hat{J}_x,\hat{J}_y,\hat{J}_z$,

$$\begin{aligned}\hat{J}_{x'} &= \hat{J}_x,\\ \hat{J}_{y'} &= \hat{J}_y\cos\theta - \hat{J}_z\sin\theta,\\ \hat{J}_{z'} &= \hat{J}_z\cos\theta + \hat{J}_y\sin\theta,\end{aligned} \tag{11}$$

one obtains the expression

$$\begin{aligned}\frac{\hat{H}^{(1)}_{\mathrm{rot}}}{hc} &= (A\cos^2\theta + B\sin^2\theta)\hat{J}^2_z + (A\sin^2\theta + B\cos^2\theta)\hat{J}^2_y\\ &\quad + C\hat{J}^2_x + (A-B)\cos\theta\sin\theta(\hat{J}_z\hat{J}_y + \hat{J}_y\hat{J}_z)\end{aligned} \tag{12}$$

for the rotational Hamiltonian in the minimum labeled 1 in Fig. 1. The Hamiltonian for minimum 2 (3) is obtained from two consecutive rotations of the axis system. First, the axes are rotated such that the hydrogen atom 2 (3) lies in the yz plane. The axis system is then rotated around the new x axis such that the axes coincide with the principal axes of rotation of the distorted structure. The rotational constants A,B,C and the angle θ which are common to the minima 1,2,3 are calculated from the experimental structure of $CH_2D_2^+$ determined in Ref. 19 and confirmed in Ref. 21 and can be adjusted to reproduce the observed rovibronic structure. One can indeed expect a slight adjustment to be necessary because the experimental structures are slightly different for the different isotopomers (and even the two isomers of CH_3D^+ or CD_3H^+) because of vibrational averaging. This treatment neglects Coriolis interactions, an approximation that is justifiable because the large distortion and the appreciable barriers tend to suppress the electronic and vibrational angular momenta.

TABLE I. Reverse correlation table of irreducible representations of the C_s point group to the $C_{3v}(M)$ molecular symmetry group.

C_s	$C_{3v}(M)$
A'	$A_1 \oplus E$
A''	$A_2 \oplus E$

The tunneling-rotation problem is set up in the product basis

$$\phi_{n,JK} = |n\rangle|\chi_n\rangle|JK\rangle, \tag{13}$$

where $|n\rangle$ and $|\chi_n\rangle$ have been defined above and $|JK\rangle$ are symmetric top rotational basis functions with J the total angular momentum quantum number and K the quantum number associated with its projection on the z axis. The Jahn-Teller distortion is sufficiently large that the vibronic angular momenta are expected to be quenched. The same is true for spin-orbit interactions and their effects on the rotational structure.

The tunneling-rotation Hamiltonian is defined as

$$\hat{H}_{\mathrm{rve}} = \hat{H}_{\mathrm{vib}} + \hat{H}_{\mathrm{rot}}, \tag{14}$$

and its matrix elements in the basis $\phi_{n,JK}$ are given by

$$\begin{aligned}H_{ij,JKJ'K'} &= \langle i|j\rangle(\langle\chi_i|\hat{H}_{\mathrm{vib}}|\chi_j\rangle\langle JK|J'K'\rangle\\ &\quad + \langle\chi_i|\chi_j\rangle\langle JK|\hat{H}_{\mathrm{rot}}|J'K'\rangle)\\ &= \langle i|j\rangle(\langle\chi_i|\hat{H}_{\mathrm{vib}}|\chi_j\rangle\delta_{JJ'}\delta_{KK'}\\ &\quad + \delta_{ij}\langle JK|\hat{H}_{\mathrm{rot}}|J'K'\rangle)\\ &= \begin{cases}\langle\chi_i|\hat{H}_{\mathrm{vib}}|\chi_j\rangle\delta_{JJ'}\delta_{KK'} + \langle JK|\hat{H}^{(i)}_{\mathrm{rot}}|J'K'\rangle & \text{for } i=j\\ \langle i|j\rangle\langle\chi_i|\hat{H}_{\mathrm{vib}}|\chi_j\rangle\delta_{JJ'}\delta_{KK'} & \text{for } i\neq j,\end{cases}\end{aligned} \tag{15}$$

where the overlap between the vibrational basis functions $\langle\chi_i|\chi_j\rangle$ has been set to 0 for $i\neq j$. The diagonalization of this matrix provides the tunneling-rotation eigenvalues and eigenvectors.

IV. RESULTS

A. Symmetry analysis and correlation diagrams

The analysis of the consequences of tunneling on the rovibronic levels is most transparent in a group-theoretical formalism. As shown previously for CH_4^+ and CD_4^+,[21] the rovibronic symmetries of the molecular levels in the presence of tunneling can be predicted using correlation tables. We first assume that the barrier separating the minima is so high that the tunneling splittings are not resolved. In this case, the rovibronic levels can be classified in the point group corresponding to the distorted structures. The minimum energy structures of CH_3D^+ and CD_3H^+ have C_s symmetry. The singly occupied molecular orbital is symmetric with respect to the reflection in the plane containing the long C–H(D) bonds and antisymmetric with respect to the plane containing the short bonds. Therefore, the electronic symme-

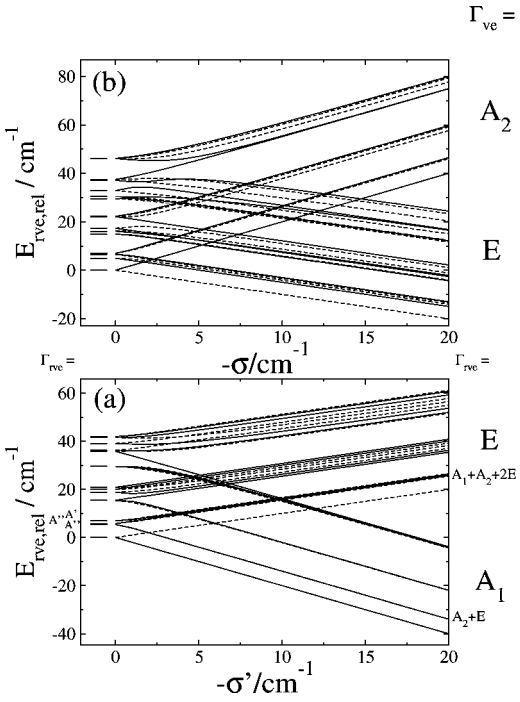

FIG. 5. Correlation diagram of the eigenvalues of the tunneling-rotation Hamiltonian (14) as a function of the tunneling integral σ for $CD_3H_\ell^+$ [panel (a)] and $CD_3H_s^+$ [panel (b)]. In the limit $\sigma=\sigma'=0$, all levels are threefold degenerate and coincide with the pattern of an asymmetric top which is depicted on the left-hand side. The full lines correspond to levels of rovibronic symmetry A_1 or A_2 in the $C_{3v}(M)$ group, whereas the dashed lines correspond to levels of symmetry E. The vibronic symmetries of the tunneling sublevels are indicated on the right-hand side of the figure by large capital letters.

tries in the ground state of $CH_3D_s^+$ and $CH_3D_\ell^+$ are A'' and A', respectively. Similarly, $CD_3H_\ell^+$ has an electronic ground state of symmetry A' and $CD_3H_s^+$ has an A'' ground state. The tunneling between the three equivalent minima (1,2,3) or (4,5,6) in Fig. 1 for each of these isomers results in a splitting of the vibronic ground state into two sublevels. The symmetry of these sublevels is then predicted by correlating the vibronic symmetry from the C_s point group to $C_{3v}(M)$, which is the appropriate molecular symmetry group in the presence of tunneling. The corresponding correlation, which is given in Table I, predicts that the tunneling leads to a doubly degenerate state (E) and a nondegenerate one (A_1 or A_2). The ordering of these tunneling levels, however, is not determined by group theory and can only be obtained from a quantitative model including the geometric phase. The method introduced in Sec. III predicts that in $CH_3D_s^+$ the lower tunneling level has the vibronic symmetry E and the upper level is of A_2 symmetry, whereas $CH_3D_\ell^+$ has an A_1 lower level and an upper level of symmetry E. $CD_3H_\ell^+$ and $CD_3H_s^+$ have the same sequence of tunneling levels as $CH_3D_\ell^+$ and $CH_3D_s^+$, respectively.

Figure 5(a) represents the eigenvalues of the tunneling-rotation Hamiltonian H_{rve} for the calculated rotational constants of $CD_3H_\ell^+$ given in Table II as a function of the tunneling integral $|\sigma'|=\delta/3$ [see Eqs. (9a)–(9d)]. In the limit $\sigma'=0$, the level pattern of an asymmetric top is obtained, each level being triply degenerate. This limit corresponds to the case of an infinite barrier that suppresses tunneling between the equivalent minima. In the case of a large tunneling splitting corresponding to a fast pseudorotational motion, two distinct stacks of rotational levels are obtained. The lower stack corresponds to a level of vibronic symmetry A_1 with a wave function that has equal amplitudes in all three minima; this level therefore possesses a simple rotational structure. In the particular case of $CD_3H_\ell^+$ the rotational structure is very close to that of a spherical top because a specific relation between the rotational constants and the tilt angle θ is accidentally fulfilled and results in an isotropic inertial tensor in the limit of fast pseudorotation. The upper stack of rotational levels exhibits a complex rotational structure and corresponds to a vibronic level of symmetry E. This state has a more complicated structure because its two components have different amplitudes in the three minima. The correlation diagram for $CD_3H_s^+$ is shown in Fig. 5(b). Two main differences to Fig. 5(a) can be seen. First, the ordering of the tunneling levels is inverted, the degenerate vibronic level now lying below the nondegenerate one. Second, the rotational structure of the nondegenerate level has a normal oblate top rotational structure in the limit of fast pseudorotation. The correlation diagrams for $CH_3D_\ell^+$ and $CH_3D_s^+$ are similar, with the difference that the rotational structure of the

TABLE II. Constants calculated using the experimental structure of $CH_2D_2^+$ determined in Ref. 19 and adjusted to reproduce the experimental spectra. A, B, C are the asymmetric top rotational constants, θ is the angle by which the z axis has been tilted away from the symmetric top principal axis in the rotation of the axis system, $\delta=3|\sigma|$ is the tunneling splitting, IE is the adiabatic ionization energy of the more stable isomer, and ZPED is the zero-point energy difference between the two isomers.

Isomer		A (cm^{-1})	B (cm^{-1})	C (cm^{-1})	θ (°)	δ (cm^{-1})	IE (hc cm^{-1})	ZPED (hc cm^{-1})
$CH_3D_s^+$	Calc.	5.68	4.22	3.03	22.2			
	Expt.	5.63(5)	4.08(10)	3.14(4)	22.2[a]	9.5(6)	101 802.8(15)	
$CH_3D_\ell^+$	Calc.	6.13	3.76	3.13	17.7			114[b]
	Expt.	6.08(6)	3.70(6)	3.11(2)	17.7[a]	6.6(5)		120.9(10)
$CD_3H_\ell^+$	Calc.	3.67	3.26	2.13	50.0			
	Expt.	3.76(9)	3.17(12)	2.21(6)	50.0[a]	1.2(6)	102 021.4(20)	
$CD_3H_s^+$	Calc.	4.29	2.70	2.29	11.4			107[b]
	Expt.	4.35(5)	2.74(6)	2.26(4)	11.4[a]	1.8(4)		122.3(20)

[a]Unchanged.
[b]*Ab initio* value at the CCSD(T)/cc-pVTZ level of theory.

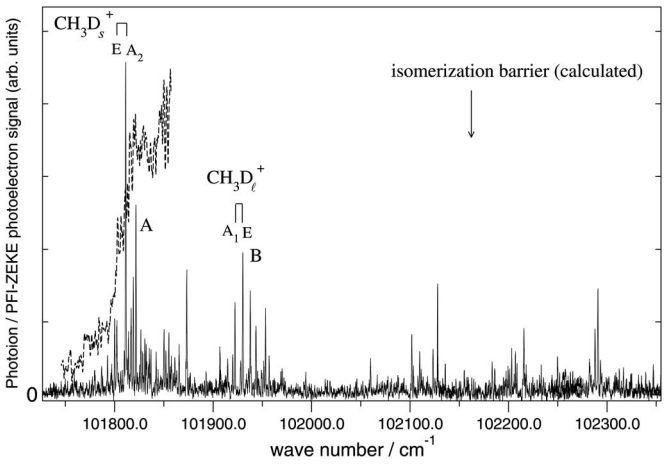

FIG. 6. PFI-ZEKE photoelectron spectrum (full line) and photoionization spectrum (dashed line) of CH_3D. The PFI-ZEKE photoelectron spectrum was recorded using a sequence of pulsed electric fields of +35 and −130 mV cm^{-1}. The position of the zero-point-corrected *ab initio* barrier for isomerization is indicated by an arrow.

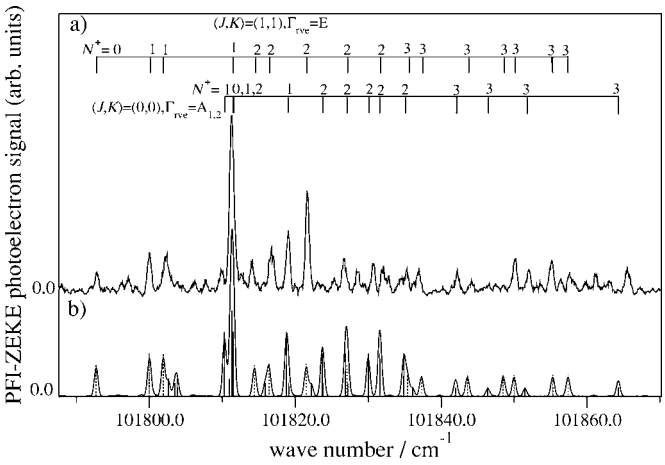

FIG. 7. Lowest band in the PFI-ZEKE photoelectron spectrum of CH_3D corresponding to isomer $CH_3D_s^+$ [trace (a)] and simulation [trace (b)]. The PFI-ZEKE photoelectron spectrum was recorded using a sequence of pulsed electric fields of +35 and −130 mV cm^{-1}. Trace (b) shows a theoretical stick spectrum consisting of transitions to levels of rovibronic symmetry A_1 or A_2 (full sticks) and transitions to levels of rovibronic symmetry E (dotted sticks). The stick spectrum has been convoluted with a Gaussian line shape of 0.6 cm^{-1} FWHM.

lower tunneling level of $CH_3D_\ell^+$ does not show the accidental "spherical top" level structure seen in Fig. 5(a).

The rovibronic symmetries of the rotationally excited levels under the effect of tunneling can also be predicted from group theory as found previously.[21] In the limit $\sigma=0$, the three $J=1$ asymmetric top levels have the rovibronic symmetries A'' $(J_{K_aK_c}=1_{01})$, A'' (1_{11}), and $A'(1_{10})$) which correlate with $A_2\oplus E$, $A_2\oplus E$, and $A_1\oplus E$, respectively. This prediction is confirmed by the tunneling-rotation calculations displayed in Fig. 5.

B. CH_3D^+

An overview of the photoionization (dashed line) and PFI-ZEKE photoelectron (full line) spectra of CH_3D near the adiabatic ionization threshold is shown in Fig. 6. The coincidence of a sharp increase in the photoionization yield from a value of zero at ~101 800 cm^{-1} with the first band (labeled A) in the PFI-ZEKE photoelectron spectrum indicates a transition to the vibrationless ground state of CH_3D^+. The following band (labeled B) in the PFI-ZEKE spectrum lies only 121 cm^{-1} higher and possesses a rotational structure that is very different from the lowest band. Beyond 102 100 cm^{-1}, the spectrum cannot be described by isolated bands any longer. This situation is reminiscent of CH_4^+ where only the lowest band can be identified as isolated spectral structure, an observation which reflects the flatness of the potential energy surface and the resultant large-amplitude motion and overlapping spectral structures at higher internal energies.

The results of the analysis of the two lowest bands of the PFI-ZEKE spectrum of CH_3D are shown in more detail in Figs. 7 and 8. In the analysis of these spectra, we have used the calculated rotational constants given in Table II and have adjusted the tunneling integral σ (or σ') until a good agreement was reached. The transitions were then assigned on the basis of the calculations, and the rotational constants, the tunneling integral, and the band center were refined in a nonlinear least-squares fitting procedure. The constants obtained in the fit are also given in Table II below the calculated values. The band centers were transformed into an adiabatic ionization energy (IE) for the more stable isomer and a zero-point energy difference (ZPED) for the less stable isomer after correcting for the field-induced shift of the ionization thresholds. The transition wave numbers were calculated using the rotational constants $A_0=5.2508$ cm^{-1} and $B_0=3.8802$ cm^{-1} for the ground electronic state of the neutral molecule from Ref. 27 and assuming that nuclear spin symmetry is conserved in the photoionizing transitions. For the calculation of the intensities, we have used a Boltzmann distribution with a rotational temperature of 7 K for both nuclear spin isomers and the same weighting factors for the different rotational branches, as used in previous studies of isotopomers of the methane cation.[19,21] The spin-statistical

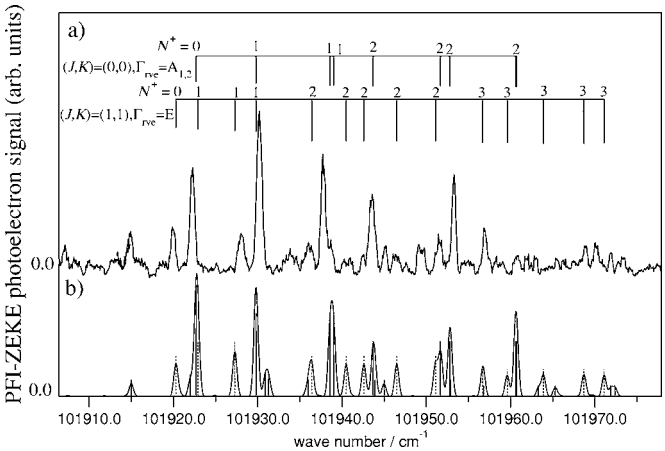

FIG. 8. Second lowest band in the PFI-ZEKE photoelectron spectrum of CH_3D corresponding to isomer $CH_3D_\ell^+$ [trace (a)] and simulation [trace (b)]. The PFI-ZEKE photoelectron spectrum was recorded using a sequence of pulsed electric fields of +35 and −130 mV cm^{-1}. Trace (b) shows a theoretical stick spectrum consisting of transitions to levels of rovibronic symmetry A_1 or A_2 (full sticks) and transitions to levels of rovibronic symmetry E (dotted sticks). The stick spectrum has been convoluted with a Gaussian line shape of 0.6 cm^{-1} FWHM.

TABLE III. Measured line positions ($\tilde{\nu}_{obs}$) and deviations from the calculated line positions ($\tilde{\nu}_{calc}-\tilde{\nu}_{obs}$) of the origin band of the CH_3D^+ $\tilde{X}\leftarrow CH_3D$ $\tilde{X}$ photoionizing transition of CH_3D. Γ_{ve}, Γ_{rve}, and Γ^+_{rve} represent the vibronic and the rovibronic symmetries in the molecular symmetry group $C_{3v}(M)$ for the neutral and the ionic states, respectively.

CH_3D ($\Gamma_{ve}=A_1$)			CH_3D^+			
Γ_{rve}	J	K	Γ^+_{rve}	N^+	$\tilde{\nu}_{obs}$ (cm^{-1})[a]	($\tilde{\nu}_{calc}-\tilde{\nu}_{obs}$) ($cm^{-1}$)
				$CH_3D^+_s$		
E	1	1	E	0	101 792.8	−0.11
E	1	1	E	1	101 799.8	0.22
E	1	1	E	1	101 802.2	−0.33
A_1	0	0	A	1	101 809.9	0.43
A_1	0	0	A	1	101 809.5–101 811.7	
E	1	1	E	1		
A_1	0	0	A	0		
A_1	0	0	A	1		
A_1	2	0	A	2		
A_2	1	0	A	1		
A_2	1	0	A	2	101 816.74	−0.83
E	1	1	E	2	101 814.0	0.40
E	1	1	E	2	101 816.6	−0.26
A_1	0	0	A	1	101 819.04	−0.29
A_2	1	0	A	2	101 819.04	0.09
E	1	1	E	2	101 821.5	−0.02
E	1	1	E	2	101 826.7[b]	0.32
E	1	1	E	2	101 830.7[b]	
E	1	1	E	2	101 832.0[b]	−0.40
E	1	1	E	3	101 835.6[b]	−0.20
E	1	1	E	3	101 836.9[b]	0.35
A_2	1	0	A	3	101 842.21	−0.30
E	1	1	E	3	101 850.15[b]	−0.15
E	1	1	E	3	101 855.2[b]	0.10
E	1	1	E	3	101 857.6[b]	−0.21
A_2	1	0	A		101 865.6	
				$CH_3D^+_\ell$		
E	2	2	E	1	101 907.0	
A_2	1	0	A	0	101 914.8	0.20
E	1	1	E	0	101 920.0	0.31
A_1	0	0	A	0	101 922.23	0.51
A_2	1	0	A	1	101 922.23	−0.20
E	1	1	E	1	101 928.0	−0.68
A_1	0	0	A	1	101 930.2	−0.45
E	1	1	E	1	101 930.2	−0.38
E	1	1	E	2	101 936.06	0.30
A_1	0	0	A	1	101 937.75	0.81
A_1	0	0	A	1	101 937.75	1.21
A_1	0	0	A	2	101 943.56	0.17
A_1	0	0	A	2	101 953.50[b]	−0.73
E	1	1	E	3	101 956.94[b]	−0.26
E	1	1	E	3	101 968.86[b]	−0.20
E	1	1	E	3	101 970.16[b]	0.92

[a]Measured transition wave numbers without correction for the field-induced shift of the ionization thresholds.
[b]Assignment tentative.

weights were also included. The weights of transitions corresponding to the emission of even and odd photoelectron partial waves were chosen to be equal. Table III lists the measured wave numbers of the transitions in both bands, their assignments, and the deviation between the measured and calculated positions.

In the spectra of the lowest band shown in Fig. 7, the agreement between observed and calculated level positions is good in the lower half of the spectrum (see also upper part of Table III). The strongest line (at 101 811 cm^{-1}) corresponds to a cluster of primarily Q type transitions, i.e., transitions with $N^+-J=0$. The assignment bars label transitions from the $(J,K)=(0,0)$ and $(1,1)$ levels of the ground state. The three lines below and the four lines above the Q branch are reproduced well by the calculation and suffice to define the tunneling splitting. If the tunneling splitting were negligible,

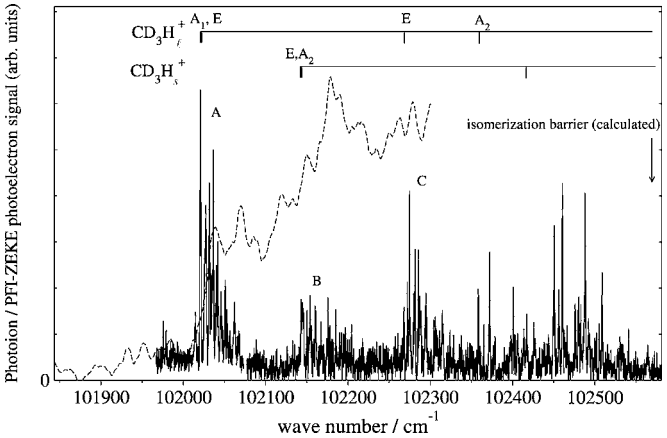

FIG. 9. PFI-ZEKE photoelectron spectrum (full line) and photoionization spectrum (dashed line) of CD_3H. The PFI-ZEKE photoelectron spectrum was recorded using a sequence of pulsed electric fields of +26 and −138 mV cm^{-1}. The position of the zero-point-corrected *ab initio* barrier for isomerization is indicated by an arrow.

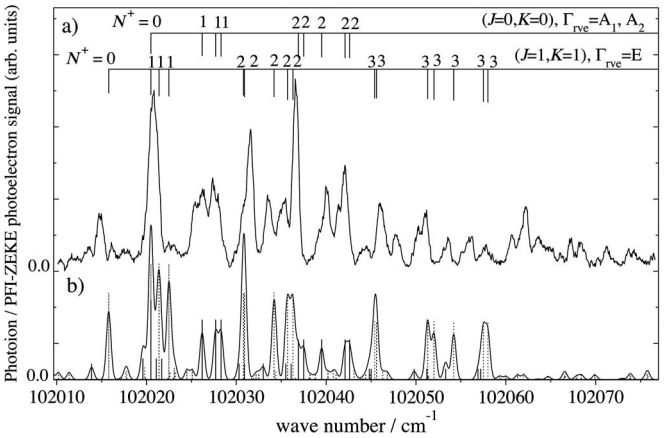

FIG. 10. Lowest band in the PFI-ZEKE photoelectron spectrum of CD_3H corresponding to isomer $CD_3H^+_\ell$ [trace (a)] and simulation [trace (b)]. The PFI-ZEKE photoelectron spectrum was recorded using a sequence of pulsed electric fields of +26 and −86 mVcm^{-1}. Trace (b) shows a theoretical stick spectrum consisting of transitions to levels of rovibronic symmetry A_1 or A_2 (full sticks) and transitions to levels of rovibronic symmetry E (dotted sticks). The stick spectrum has been convoluted with a Gaussian line shape of 0.6 cm^{-1} FWHM.

an additional line would be observed to the higher wave number side of the pair of lines around 101 801 cm^{-1}. Transitions from $(J,K)=(0,0)$ to the upper tunneling component of $N^+=0$ and to the two lower tunneling components of $N^+=1$ nearly coincide and form the strong line cluster around 101 811 cm^{-1}. The pair of lines around 101 801 cm^{-1} is assigned to the transition from $(J,K)=(1,1)$ to the lower tunneling component of $N^+=1$ and the transition to the upper component is also located close to 101 811 cm^{-1}. The agreement between calculated and observed intensities is, however, less satisfactory. Although the lower part of the spectrum is well reproduced, the intensities are clearly overestimated by the calculation in the upper half. However, given the crude model used to calculate the intensities (see above), the agreement between the calculated and measured intensities can be regarded as satisfactory.

The second band of the PFI-ZEKE photoelectron spectrum of CH_3D and its simulation are shown in Fig. 8. The agreement between calculated and observed line positions is again good for the strongest transitions (see the lower part of Table III). As in the spectrum of the lower band, the intensities are also overestimated on the high wave number side of the spectrum.

In the simulation of all spectra of CH_3D^+ we were led to reduce the intensity of transitions originating from levels of rovibronic symmetry E by a factor of 2 compared to those originating from A_1 or A_2 levels. This observation might originate from a partial conversion of nuclear spin symmetries in the collisional cooling process.

C. CD_3H^+

The photoionization and PFI-ZEKE photoelectron spectra of CD_3H (dashed and full lines, respectively) over the range 101 900–102 600 cm^{-1} are displayed in Fig. 9. The lowest band of the PFI-ZEKE photoelectron spectrum (labeled A) coincides with the onset of the photoionization signal and is therefore assigned to the adiabatic ionization threshold of CD_3H. In the PFI-ZEKE photoelectron spectrum of CD_3H^+, at least three isolated bands can be identified. The first and third bands (labeled A and C) have a similar rotational structure which differs from that of the second (labeled B). The band labeled C and the spectral lines around 102 370 cm^{-1} can be tentatively assigned to excited pseudorotational levels of the $CD_3H^+_\ell$ isomer. As expected the level of vibronic symmetry E (associated with band C) lies below the A_2 level. At higher energies, the simple band structure of the spectrum is lost, which is another indication of the flatness of the potential energy surface at higher energies. The group of lines beyond 102 400 cm^{-1} could possibly be assigned to a strongly perturbed band.

The separation between the two lowest bands amounts to approximately 120 cm^{-1} as in the spectrum of CH_3D^+. The analysis of the two lowest bands was performed in the same way as for the spectra of CH_3D^+. For the calculation of the transition wave numbers we have used the rotational constants $B_0=3.27\,916$ cm^{-1} and $C_0=2.62\,896$ cm^{-1} for the ground vibronic level of CD_3H from Ref. 28 and assumed that nuclear spin symmetry is conserved in the photoelectron transitions. The intensities were simulated assuming a rotational temperature of 7 K and using the same weighting factors for different rotational branches and the same procedure as for CH_3D^+ (see above). We have assumed that nuclear spin symmetry is conserved in the collisional cooling of the CD_3H molecules.

The spectrum of the lowest band and its simulation using the constants for $CD_3H^+_\ell$ reported in Table II are compared in Fig. 10. The general structure of the band and most lines are reproduced by the simulation. The signal-to-noise ratio of the spectra of CD_3H is poorer than that of the spectra of CH_3D (compare Figs. 6 and 9), which unfortunately makes the analysis of the rotational structure more difficult. The transitions to the rotational levels of the lower tunneling component of vibronic symmetry A_1 are located at 102 020 cm^{-1} $(N^+=0)$, 102 027 cm^{-1} $(N^+=1)$, and 102 034 cm^{-1} $(N^+=2)$ and those to the upper tunneling component of symmetry E are located at 102 021 cm^{-1} $(N^+=1)$ and 102 037 cm^{-1}

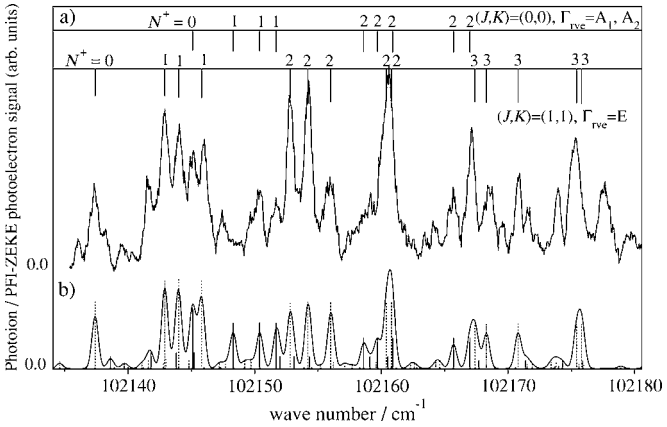

FIG. 11. Second lowest band in the PFI-ZEKE photoelectron spectrum of CD_3H corresponding to isomer $CD_3H_s^+$ [trace (a)] and simulation [trace (b)]. The PFI-ZEKE photoelectron spectrum was recorded using a sequence of pulsed electric fields of +26 and −86 mV cm^{-1}. Trace (b) shows a theoretical stick spectrum consisting of transitions to levels of rovibronic symmetry A_1 or A_2 (full sticks) and transitions to levels of rovibronic symmetry E (dotted sticks). The stick spectrum has been convoluted with a Gaussian line shape of 0.6 cm^{-1} FWHM.

($N^+=2$). Deviations between the calculated and observed line distributions are, however, observed. We cannot entirely exclude the possibility that impurities in the CD_3H sample (mostly CH_3Cl, CH_3F), though present in traces only, may have contributed weakly to the PFI-ZEKE photoelectron spectrum. Because of these deviations, many rotational assignments of this band must be regarded as tentative.

The agreement between calculated and experimental spectra is better for the second band of the PFI-ZEKE spectrum, which is shown in more detail in Fig. 11. The constants used for the calculation are listed in Table II for $CD_3H_s^+$. In this simulation, line positions (Table IV) and intensities are reproduced satisfactorily and the assignment of all strong transitions is unambiguous. The transitions to the rotational levels of the lower tunneling component of vibronic symmetry E are located at 102 137 cm^{-1} ($N^+=0$), 102 143 cm^{-1} ($N^+=1$), and 102 153 cm^{-1} ($N^+=2$) and those to the upper tunneling component of symmetry A_2 are located at 102 145 cm^{-1} ($N^+=0$), 102 153 cm^{-1} ($N^+=1$), and 102 167 cm^{-1} ($N^+=2$).

V. DISCUSSION

The analysis of the rotational structure of the lowest two bands of the PFI-ZEKE spectra of CH_3D^+ and CD_3H^+ leads to several important conclusions. First, the ordering of the vibronic levels enables the identification of two distinct isomers of both CH_3D^+ and CD_3H^+. Second, the rotational constants allow an unambiguous identification of each band with one of the isomers of CH_3D^+ and CD_3H^+. This form of isomerism of a polyatomic molecule subject to a JT effect results from isotopic substitution and has not been observed previously. These assignments are supported by *ab initio* quantum chemical calculations which predict the isomer $CH_3D_s^+$ to be more stable than the isomer $CH_3D_\ell^+$ by 114 cm^{-1} (see Table II) and the isomer $CD_3H_\ell^+$ to be more stable than the isomer $CD_3H_s^+$ by 107 cm^{-1}, in good agreement with the experimental values. The good agreement with the predicted rotational constants (see Table II) also supports the results of the present analysis.

In addition to the structural parameters, the present analysis also provides information on the topology of the potential energy surfaces and the tunneling dynamics. In the adjustment of the tunneling integrals, σ and σ' were found to be negative for both CH_3D^+ and CD_3H^+, thus confirming the ordering of tunneling levels predicted in Sec. III. The analysis of the rovibronic structure of CH_3D^+ and CD_3H^+, in particular the determination of the ordering of the E and A_1 (or A_2) vibronic levels, thus constitutes an experimental determination of the location of the twofold conical intersections on the potential energy surface. The location of these conical intersections could previously only be predicted by theoretical methods.

The size of the tunneling splittings in CH_3D^+ and CD_3H^+ is consistent with the values that we have determined previously for CH_4^+ and CD_4^+. In a first approximation, one could assume that single deuteration of CH_4^+ has a negligible effect on the value of the tunneling integral σ for the isomer $CH_3D_s^+$. In CH_4^+, we have determined $\sigma=-4.1(10)$ cm^{-1} [the corresponding tunneling splitting is $\delta=4|\sigma|=16.4(40)$ cm^{-1} (Refs. 17 and 21)]. In $CH_3D_s^+$ we have obtained $\sigma=-3.2(2)$ cm^{-1} and a corresponding tunneling splitting $\delta=3|\sigma|$ of 9.5(6) cm^{-1}. The values of the tunneling integral in CH_4^+ and CH_3D^+ are thus similar, as expected, and the difference in the tunneling splittings results primarily from the ratio $\delta(CH_4^+)/\delta(CH_3D^+)\approx 4/3$ imposed by the topology. The smaller value of the tunneling integral in CH_3D^+ can be understood from the increased reduced mass associated with the pseudorotational motion. The zero-point-corrected barrier heights were calculated from the purely electronic barrier height of 1014 cm^{-1} [at the CCSD(T)/cc-pVTZ level[21]] by subtracting the harmonic zero-point energy difference between the minimum energy structure of $CH_3D_s^+$ and the saddle-point structure. The zero-point energy of the saddle-point structure was calculated by omitting the imaginary frequency from the zero-point energy sum. The values listed in Table V show that the zero-point-corrected barrier height for the pseudorotational motion of $CH_3D_s^+$ is smaller than that in $CH_3D_\ell^+$, which explains the smaller value of the tunneling splitting [$\delta=6.6(5)$ cm^{-1}] found for this isomer.

The tunneling motion in CD_3H^+ involves three deuterium atoms instead of three hydrogen atoms and should therefore be characterized by tunneling integrals of similar magnitude as in CD_4^+. For CD_4^+, we have previously determined the value $\sigma=0.35(10)$ cm^{-1}.[21] The tunneling integral [$\sigma=-0.4(1)$ cm^{-1}] for $CD_3H_\ell^+$ is equal to that of CD_4^+ within the experimental error, whereas that for $CD_3H_s^+$ [$\sigma=-0.6(1)$ cm^{-1}] is slightly larger. The zero-point-corrected barrier height for the pseudorotational motion is similar for $CD_3H_\ell^+$ than for $CD_3H_s^+$ (see Table V). One can therefore expect the tunneling integral of $CD_3H_\ell^+$ to be similar to that of $CD_3H_s^+$, which is indeed in agreement with the experimental results. The values of the tunneling integrals are thus compatible with *ab initio* quantum chemical calculations.

The number of isolated bands that can be identified by simple inspection of the PFI-ZEKE photoelectron spectra increases from 1 in CH_4^+ to 2 in CH_3D^+ and 3 in CD_3H^+. This

TABLE IV. Measured line positions ($\tilde{\nu}_{obs}$) and deviations from the calculated line positions ($\tilde{\nu}_{calc}-\tilde{\nu}_{obs}$) of the origin band of the CD_3H^+ $\tilde{X}\leftarrow CD_3H$ $\tilde{X}$ photoionizing transition of CD_3H. Γ_{ve}, Γ_{rve}, and Γ^+_{rve} represent the vibronic and the rovibronic symmetries in the molecular symmetry group $C_{3v}(M)$ for the neutral and the ionic states, respectively.

CD_3H ($\Gamma_{ve}=A_1$)			CD_3H^+			
Γ_{rve}	J	K	Γ^+_{rve}	N^+	$\tilde{\nu}_{obs}$ (cm^{-1})[a]	($\tilde{\nu}_{calc}-\tilde{\nu}_{obs}$) ($cm^{-1}$)
				$CD_3H^+_\ell$		
A_2	1	0	A	0	102 014.86	−0.40
A_1	0	0	A	0	102 020.75	0.27
E	1	1	E	1	102 020.75	0.26
A_1	0	0	A	1	102 026.70	0.01
A_1	0	0	A	1	102 027.80	0.36
E	1	1	E	2	102 031.54	−0.12
A_2	1	0	A	2	102 033.60[b]	−0.09
E	1	1	E	2	102 035.22[b]	−0.47
E	1	1	E	2	102 036.60[b]	−0.40
E	1	1	E	2	102 036.60[b]	0.17
A_1	0	0	A	2	102 040.08[b]	−0.08
E	1	1	E	3	102 046.06[b]	0.02
A_2	1	0	A	3	102 053.55[b]	0.24
				$CD_3H^+_s$		
E	1	1	E	0	102 137.40	−0.01
A_2	1	0	A	1	102 141.60	0.17
E	1	1	E	1	102 142.92	0.01
E	1	1	E	1	102 144.02	−0.01
A_1	0	0	A	0	102 145.09	0.06
E	1	1	E	1	102 145.97	−0.21
A_1	0	0	A	1	102 150.37	0.01
A_1	0	0	A	1	102 151.69	0.03
E	1	1	E	2	102 152.79	−0.04
E	1	1	E	2	102 154.22	−0.03
E	1	1	E	2	102 155.92	0.02
E	1	1	E	2	102 160.53	−0.19
E	1	1	E	2	102 160.53	0.30
A_1	0	0	A	2	102 165.64	0.04
A_1	0	0	A	2	102 167.10	−0.10
E	1	1	E	3	102 167.10	0.24
E	1	1	E	3	102 168.53	−0.27
E	1	1	E	3	102 170.83	−0.08

[a]Measured transitions without field correction.
[b]Assignment tentative.

observation can also be attributed to the zero-point effects and the usual effects associated with the substitution of a light by a heavier isotope. The largest number of localized bands is actually observed in CD_4^+ but their analysis was rendered difficult by the low signal-to-noise ratio of the PFI-ZEKE spectra.[21] Above the barrier hindering the pseudorotational motion, the configuration space accessible to the nuclear wave function increases strongly because the barriers separating the equivalent structures of one isomer are similar to those separating structures of the two isomers. At the internal energies where pseudorotation is no longer hindered, it is thus generally impossible to distinguish the two isomers from each other, because the nuclear wave functions start spreading over the configurational space associated with both isomers and isomerization takes place. For simplicity, we consider levels of CH_3D^+ or CD_3H^+ corresponding to a zero total angular momentum. The lowest levels of $CH_3D^+_s$ and $CH_3D^+_\ell$ are of vibronic symmetries E and A_1 and A_2 and E, respectively. In the simple tunneling model, the A_1 and A_2 levels are completely localized in the three minima corresponding to one of the isomers, whereas the wave functions of each E level have small amplitudes in the minima of the other isomer. The matrix element connecting basis states of the isomeric structures must become irrelevant because the zero-point levels of the two isomers are not resonant. This situation is comparable to the case of the hydrogen fluoride dimer, where the rotational levels of $(HF)_2$ and $(DF)_2$ are split by the effect of tunneling but no such splitting is observed in HFDF (Ref. 29) (see also Ref. 30). In the region below the barrier, the isomers will thus only interconvert in the case of an accidental vibrational degeneracy.

The present results on CH_3D^+ and CD_3H^+ are compatible with the results of the EPR investigations of Knight *et al.*[18] who concluded that the three H (D) nuclei in CH_3D^+

TABLE V. Barrier heights at the CCSD(T)/cc-pVTZ level of *ab initio* theory after harmonic zero-point corrections. The barrier heights for pseudorotations exchanging identical nuclei are given with respect to the minima of the corresponding isomers, whereas the isomerization barriers are given with respect to the minimum of the more stable isomer. The purely electronic barrier height amounts to 1014 cm^{-1} (Ref. 21).

Isomer	Pseudorotation barrier (cm^{-1})	Isomerization barrier (cm^{-1})
$CH_3D_s^+$	333	360
$CH_3D_\ell^+$	550	
$CD_3H_\ell^+$	485	564
$CD_3H_s^+$	486	

(CD_3H^+) are equivalent, the D atom in CH_3D^+ lies in the plane perpendicular to the singly occupied (*p*-like) molecular orbital, and the H atom of CD_3H^+ lies in the plane containing the orbital axis. From the absence of a spectral signature of a second isomer in the EPR spectrum, we conclude that thermalization in the 4 K neon matrix has led to a complete conversion of the high energy to the low energy isomer.

VI. CONCLUSIONS

The analysis of the spectra of CH_3D^+ and CD_3H^+ has revealed a new kind of isotope isomerism which is expected to occur whenever vibronic coupling leads to deep equivalent minima on the potential energy surface of a polyatomic molecule. The equivalent minima of CH_4^+ form two sets of three equivalent structures each in both CH_3D^+ and CD_3H^+. These two sets are no longer isoenergetic because of different zero-point energies. Consequently, the interconversion of the isomers by tunneling is suppressed and the molecules may be isolated in one of their isomeric forms long enough to exhibit different chemical properties. For example, deuterium abstraction from $CH_3D_\ell^+$ is likely to be much faster than from $CH_3D_s^+$ because the bond energies probably differ strongly. The two isomers of CH_3D^+ and CD_3H^+ could be prepared selectively by PFI-ZEKE photoelectron spectroscopy, mass-analyzed threshold ionization spectroscopy,[31] or coincidence techniques[32] which would allow an investigation of their chemical reactivity.

The ground state of both isomers of CH_3D^+ and CD_3H^+ can be described as a tunneling doublet resulting from the fast cyclic exchange of the three equivalent atoms. The period $\tau = h/\delta$ for this motion can directly be determined from the tunneling splittings δ derived from the spectra and listed in Table II and amounts to 3.5(2) ps for $CH_3D_s^+$, 5.1(4) ps for $CH_3D_\ell^+$, 28^{+27}_{-10} ps for $CD_3H_\ell^+$, and 18^{+6}_{-3} ps for $CD_3H_s^+$. Moreover, each isomer possesses a threefold dynamical symmetry, i.e., the three H or D atoms are chemically equivalent.

The ordering of the tunneling sublevels in the two isomers of CH_3D^+ and CD_3H^+ has revealed the positions of twofold conical intersections on the potential energy surface, an information that cannot be obtained directly from the properties of CH_4^+ because of its high permutational symmetry.

In conclusion we have shown that partial isotopic substitution in polyatomic molecules not only is very helpful in understanding the dynamics and topological relationships of complex vibronic coupling problems but it even leads to a previously unknown form of isomerism of chemical relevance.

ACKNOWLEDGMENTS

The authors thank Dr. X. Qian for her experimental help in the recording of the spectrum of CD_3H and Professor M. S. Child (Oxford) and Professor G. Duxbury (Strathclyde) for useful discussions. This work is supported financially by the Swiss National Science Foundation and the ETH Zürich.

[1] I. B. Bersuker, *The Jahn-Teller Effect* (Cambridge University Press, Cambridge, 2006).
[2] *Conical Intersections: Electronic Structure, Dynamics and Spectroscopy*, Advanced Series in Physical Chemistry Vol. 15, edited by W. Domcke, D. R. Yarkony, and H. Köppel (World Scientific, Singapore, 2004).
[3] B. Scharf and J. Jortner, Chem. Phys. Lett. **2**, 68 (1968).
[4] J. Eiding and W. Domcke, Chem. Phys. **163**, 133 (1992).
[5] A. Carrington, H. C. Longuet-Higgins, R. E. Moss, and P. F. Todd, Mol. Phys. **9**, 187 (1965).
[6] R. G. Lawler, J. R. Bolton, G. K. Fraenkel, and T. H. Brown, J. Am. Chem. Soc. **86**, 521 (1964).
[7] B. Scharf, R. Vitenberg, B. Katz, and Y. B. Band, J. Chem. Phys. **77**, 2226 (1982).
[8] L. Yu, D. W. Cullin, J. M. Williamson, and T. A. Miller, J. Chem. Phys. **98**, 2682 (1993).
[9] H. C. Longuet-Higgins, U. Öpik, M. H. L. Pryce, and R. A. Sack, Philos. Trans. R. Soc. London, Ser. A **244**, 1 (1958).
[10] G. Herzberg and H. C. Longuet-Higgins, Discuss. Faraday Soc. **35**, 77 (1963).
[11] B. E. Applegate, A. J. Bezant, and T. A. Miller, J. Chem. Phys. **114**, 4869 (2001).
[12] M. N. Paddon-Row, D. J. Fox, J. A. Pople, K. N. Houk, and D. W. Pratt, J. Am. Chem. Soc. **107**, 7696 (1985).
[13] B. E. Applegate, T. A. Barckholtz, and T. A. Miller, Chem. Soc. Rev. **32**, 38 (2003).
[14] W. Meyer, J. Chem. Phys. **58**, 1017 (1973).
[15] R. F. Frey and E. R. Davidson, J. Chem. Phys. **88**, 1775 (1988).
[16] S. Zilberg and Y. Haas, J. Am. Chem. Soc. **125**, 1810 (2003).
[17] H. J. Wörner, R. van der Veen, and F. Merkt, Phys. Rev. Lett. **97**, 173003 (2006).
[18] L. B. Knight, Jr., G. M. King, J. T. Petty, M. Matsushita, T. Momose, and T. Shida, J. Chem. Phys. **103**, 3377 (1995).
[19] R. Signorell, M. Sommavilla, and F. Merkt, Chem. Phys. Lett. **312**, 139 (1999).
[20] R. Signorell and F. Merkt, Faraday Discuss. **115**, 205 (2000).
[21] H. J. Wörner, X. Qian, and F. Merkt, J. Chem. Phys. **126**, 144305 (2007).
[22] F. Merkt, A. Osterwalder, R. Seiler, R. Signorell, H. Palm, H. Schmutz, and R. Gunzinger, J. Phys. B **31**, 1705 (1998).
[23] S. D. Brossard, P. G. Carrick, E. L. Chappell, S. C. Hulegaard, and P. C. Engelking, J. Chem. Phys. **84**, 2459 (1986).
[24] H. J. Wörner (unpublished).
[25] M. V. Berry, Proc. R. Soc. London, Ser. A **392**, 45 (1984).
[26] F. S. Ham, Phys. Rev. Lett. **58**, 725 (1987).
[27] G. Tarrago, M. Delaveau, L. Fusina, and G. Guelachvili, J. Mol. Spectrosc. **126**, 149 (1987).
[28] G. Tarrago and J. Dupré-Maquaire, J. Mol. Spectrosc. **96**, 170 (1982).
[29] T. R. Dyke, B. J. Howard, and W. Klemperer, J. Chem. Phys. **56**, 2442 (1972).
[30] M. Quack and M. A. Suhm, J. Chem. Phys. **95**, 28 (1991).
[31] F. Merkt, S. R. Mackenzie, and T. P. Softley, J. Chem. Phys. **99**, 4213 (1993).
[32] C. Y. Ng, Annu. Rev. Phys. Chem. **53**, 101 (2002).